

Spin Alignment, Phase Transition and Neutral Pseudoscalar Meson Dynamics of QGP in the Presences of Magnetic and Vorticity Fields

1. The Spin Alignment and Phase Structure of Thermal QGP under Rotation
2. The Anomalous Magnetic Moment and Pseudoscalar Meson Dynamics in the Magnetized QCD Background
3. Rotation Effect on the Deconfinement Phase Transition in Holographic QCD
4. Summary and Conclusions

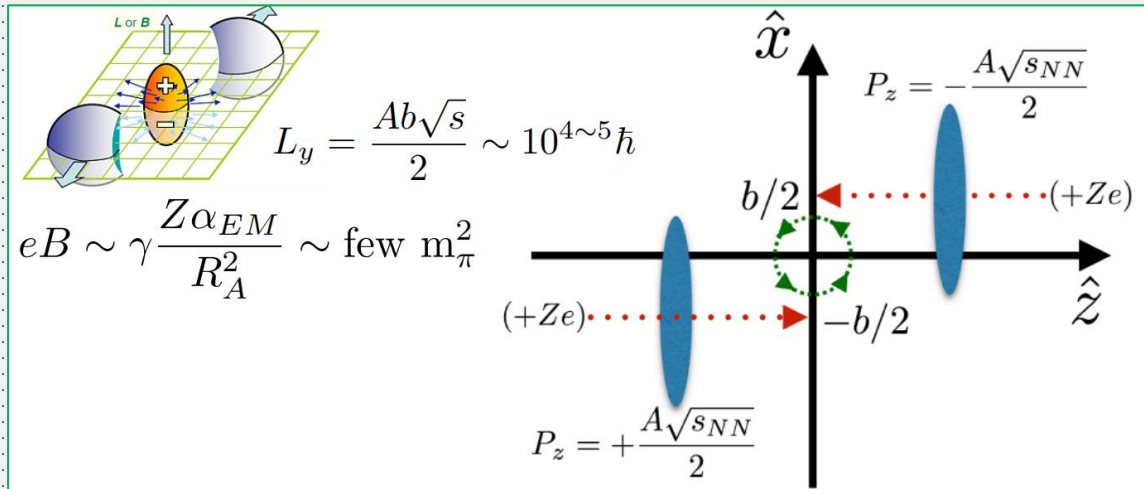
Sheng-Qin Feng (冯笙琴) (Three Gorges Univ.)

Based on:

- (1) Yang Hua (华杨) and S.-Q. Feng, Phys. Rev. D **111**, 036012 (2025);
- (2) J.-H. Wang (王嘉豪) and S.-Q. Feng, Phys. Rev. D **109**, 066019 (2024);
- (3) Yan-Ru Bao (暴彦汝) and Sheng-Qin Feng, Phys. Rev. D **109**, 096033 (2024);
- (4) Y.-W. Qiu (邱屹威) and S.-Q. Feng, Phys. Rev. D **107**, 076004 (2023);
- (5) X.-Q. Zhu (朱学强) and S.-Q. Feng, Phys. Rev. D **107**, 016018 (2023);
- (6) Y.-W. Qiu (邱屹威) and S.-Q. Feng, X.-Q. Zhu (朱学强), Phys. Rev. D **108**, 116022 (2023).
- (7) C.-Y. Yang (杨昌勇) and Sheng-Qin Feng, arXiv:2503.17056. accepted to be published in Phys. Rev. D

Extremal Vorticity and Magnetic Fields in Relativistic HIC

For a non-central collision, the dense matter produced in the overlapped region of the collision will carry a global angular momentum along the direction opposite to the reaction plane ($-\hat{y}$). Assuming that a partonic system is formed immediately following the initial collision, interactions among produced partons will lead to formation of a quark – gluon plasma (QGP) .



Vorticity fields $\omega \sim 10^{21} s^{-1}$
STAR, Nature 548 (2017) 62-65;
Becattini, Liao, Lisa,
Lect.Notes Phys. 987 (2021).

Magnetic fields $B \sim 10^{18} \text{ Gauss}$
W. T. Deng, X. G. Huang,
PRC 85, 044907 (2012).

QCD

- Phase structure
- Spin polarization
- Jet quenching
- Meson/baryon mass
- ⋮

NJL model

Quark meson model

Lattice QCD

Holographic model

⋮

1. The Spin Alignment and Phase Structure of Thermal QGP under Rotation

- (1) Yang Hua (华杨) and Sheng-Qin Feng, Phys. Rev. D **111**, 036012 (2025);
- (2) Yan-Ru Bao (暴彦汝) and Sheng-Qin Feng, Phys. Rev. D **109**, 096033 (2024).

From Gluon Topology to Quark Charality

$$Q_w = \frac{1}{32\pi^2} \int d^4x F^{a\mu\nu} \tilde{F}_{\mu\nu}^a$$

In the quark-gluon plasma (QGP), once these gluon configurations are excited at a certain spacetime point, the topological charge of the vacuum around that point will be altered by these gluon configurations. The chirality imbalance $N_5 = N_R - N_L = -2Q_w$ is induced by the nonzero topological charge through the axial anomaly of QCD.

A non-zero Q_w will induce a corresponding fluctuation in the quark chiral imbalance N_5 . This process will result in chiral imbalance between right and left quarks, leading to the violation of parity (P) and charge-parity (CP) symmetry in the thermal plasma.

The effects of a chiral imbalance in a medium can be implemented in the grand canonical ensemble by introducing a chiral chemical potential μ_5 .

- [1] J. Chao, P. Chu, and M. Huang, Phys. Rev. D 88, 054009 (2013);
- [2] Yang Hua (华杨) and S.-Q. Feng, Phys. Rev. D 111, 036012 (2025);
- [3] Yan-Ru Bao (暴彦汝) and S.-Q. Feng, Phys. Rev. D 109, 096033 (2024).

The Lagrangian of NJL model with the chiral chemical potential μ_5

The QCD matter produced in heavy-ion non-central collisions can rotate rapidly with local angular velocities ranging from 0.01 to 0.1 GeV. By considering the chiral imbalance of quark matter in a rotating background, we provide the Lagrangian of two flavors under the mean field approximation of the NJL model as:

$$L_{MFA} = \bar{\psi} \left[i\gamma^\mu \partial_\mu - M + \mu \gamma^0 + \mu_5 \gamma^0 \gamma^5 + (\gamma^0)^{-1} \left((\vec{\omega} \times \vec{x}) \cdot (-i\vec{\partial}) + \vec{\omega} \cdot \vec{S}_{4 \times 4} \right) \right] - G_s \sigma^2$$

In cylindrical coordinates, the general positive-energy solutions for the quark field from the Dirac equation corresponding to the above Lagrangian is given as

$$\psi(\theta, r) = e^{-iEt+iP_z z} \begin{pmatrix} ce^{in\theta} J_n(p_t r) \\ ide^{i(n+1)\theta} J_{n+1}(p_t r) \\ c'e^{in\theta} J_n(p_t r) \\ id'e^{i(n+1)\theta} J_{n+1}(p_t r) \end{pmatrix}$$

[1] Y. Jiang and J. Liao, Phys. Rev. Lett. 117, 192302 (2016);

[2] Yang Hua (华杨) and S.-Q. Feng, Phys. Rev. D 111, 036012 (2025)

The energy level, thermodynamic potential and chiral charge density

Through the calculation of the finite temperature field, the energy level and thermodynamic potential by rotation are obtained as follows:

$$E_{n,s} = \sqrt{\left(\sqrt{p_t^2 + p_z^2} - s\mu_5\right)^2 + M^2} - \left(n + \frac{1}{2}\right)\omega$$

$$\Omega = \frac{(M - m)^2}{4G_s} - \frac{N_f N_c}{8\pi^2} \sum_{n=-\infty}^{+\infty} \sum_{s=\pm 1} \int dp_t^2 dp_z W_{n,s} \left\{ E_{n,s} + T \ln \left[1 + e^{-\beta(E_{n,s} - u)} \right] + T \ln \left[1 + e^{-\beta(E_{n,s} + u)} \right] \right\}$$

$$W_{n,s} = [J_n^2(p_t r) + \lambda^2 J_{n+1}^2(p_t r)] / (1 + \lambda^2)$$

Gap equation: $\frac{\partial \Omega}{\partial M} = 0, \quad \frac{\partial^2 \Omega}{\partial M^2} > 0$

The chiral charge density n_5 is defined by : $n_5 = -\frac{\partial \Omega}{\partial \mu_5}$

Related theory

The **chiral charge density** we aim to study is defined by the negative partial derivative of the thermodynamic potential with respect to the chiral chemical potential:

$$n_s = -\frac{\partial \Omega}{\partial \mu_s}$$

According to the **quark recombination model [1, 2]**, the spin alignment of fermions is composed of the particle number densities of quarks and antiquarks, which is given by the partial derivative of the thermodynamic potential with respect to the chemical potential:

$$N_{\uparrow}^+ = \frac{N_f N_c}{4\pi^2} \sum_{n=-\infty}^{+\infty} \sum_{s=\pm 1} \int dp_t dp_z p_t \frac{J_n^2(p_t r)}{1+\lambda^2} \frac{e^{-\beta(E_{n,s}-\mu)}}{1+e^{-\beta(E_{n,s}-\mu)}}$$

$$N_{\downarrow}^+ = \frac{N_f N_c}{4\pi^2} \sum_{n=-\infty}^{+\infty} \sum_{s=\pm 1} \int dp_t dp_z p_t \frac{\lambda^2 J_{n+1}^2(p_t r)}{1+\lambda^2} \frac{e^{-\beta(E_{n,s}-\mu)}}{1+e^{-\beta(E_{n,s}-\mu)}}$$

$$N_{\uparrow}^- = -\frac{N_f N_c}{4\pi^2} \sum_{n=-\infty}^{+\infty} \sum_{s=\pm 1} \int dp_t dp_z p_t \frac{J_n^2(p_t r)}{1+\lambda^2} \frac{e^{-\beta(E_{n,s}+\mu)}}{1+e^{-\beta(E_{n,s}+\mu)}}$$

$$N_{\downarrow}^- = -\frac{N_f N_c}{4\pi^2} \sum_{n=-\infty}^{+\infty} \sum_{s=\pm 1} \int dp_t dp_z p_t \frac{\lambda^2 J_{n+1}^2(p_t r)}{1+\lambda^2} \frac{e^{-\beta(E_{n,s}+\mu)}}{1+e^{-\beta(E_{n,s}+\mu)}}$$

[1] Z.-T. Liang and X.-N. Wang, Phys. Rev. Lett. **94**, 102301 (2005);

[2] Z.-T. Liang and X.-N. Wang, Phys. Lett. **B 629**, 20 (2005).



Related theory

基于以上事实和已成熟的理论结果，结合QCD物质的自旋轨道耦合和手征不平衡探讨手征相变和矢量介子的自旋排列具有研究意义。

自旋极化侧重于描述粒子自旋是否朝某一特定方向偏向或被“定向”。自旋排列则更多关注粒子自旋在系统中的空间排列方式，是否有某种有序的规律。

实验上，矢量介子的自旋排列可以通过矢量介子衰变为两个赝标量粒子的衰变产物的角分布来测量：

$$\frac{dN}{d \cos \theta^*} = \frac{3}{4} [1 - \rho_{00} + (3\rho_{00} - 1) \cos^2 \theta^*]$$

在这里我们采用夸克重组合模型（夸克和反夸克的自旋极化来表示矢量介子的自旋排列）：

$$\rho_{00} = \frac{1 - P_q P_{\bar{q}}}{3 + P_q P_{\bar{q}}} \quad \rho_{00} \approx \frac{1}{3} - \frac{4}{9} P_q P_{\bar{q}}$$

- [1] K. Schilling. and P. Seyboth, and E. W. Guenter. On the Analysis of Vector Meson Production by Polarized Photons. Nucl. Phys. B 15, 397 (1970).
- [2] Z.-T. Liang, and X.-N. Wang, Globally polarized quark-gluon plasma in non-central A + A collisions. Phys. Rev. Lett 94, 102301(2005).



Related theory

夸克的自旋极化由夸克和反夸克粒子数密度组成：

$$P_q = \frac{N_{\uparrow}^+ - N_{\downarrow}^+}{N_{\uparrow}^+ + N_{\downarrow}^+}, P_{\bar{q}} = \frac{N_{\uparrow}^- - N_{\downarrow}^-}{N_{\uparrow}^- + N_{\downarrow}^-}$$

然后， ρ 矢量介子的自旋排列可以近似地表示为：

$$\rho_{00} = \frac{1}{3} - \frac{4}{9} \frac{N_{\uparrow}^+ - N_{\downarrow}^+}{N_{\uparrow}^+ + N_{\downarrow}^+} \frac{N_{\uparrow}^- - N_{\downarrow}^-}{N_{\uparrow}^- + N_{\downarrow}^-}$$

矢量介子的自旋取决于组成夸克的自旋密度，但不依赖于自旋极化的符号，即，自旋向上夸克的数量是否超过自旋向下夸克或反之亦然，可以获得相同的自旋排列。

[1]F. Sun, and J. Shao and R. Wen and K. Xu and M. Huang, Chiral phase transition and spin alignment of vector mesons in the polarized-Polyakov-loop Nambu–Jona-Lasinio model under rotation. Phys. Rev. D 109, 116017 (2024);

[2]K. Xu and M. Huang, Spin alignment of vector mesons induced by local spin density fluctuations. Phys. Rev. D 110, 094034 (2024).

Numerical Results

When studying the spin alignment of vector mesons, besides our quark recombination model, there is also the **quark condensation model [1]**. The spin alignment corresponding to vector mesons can take the following form

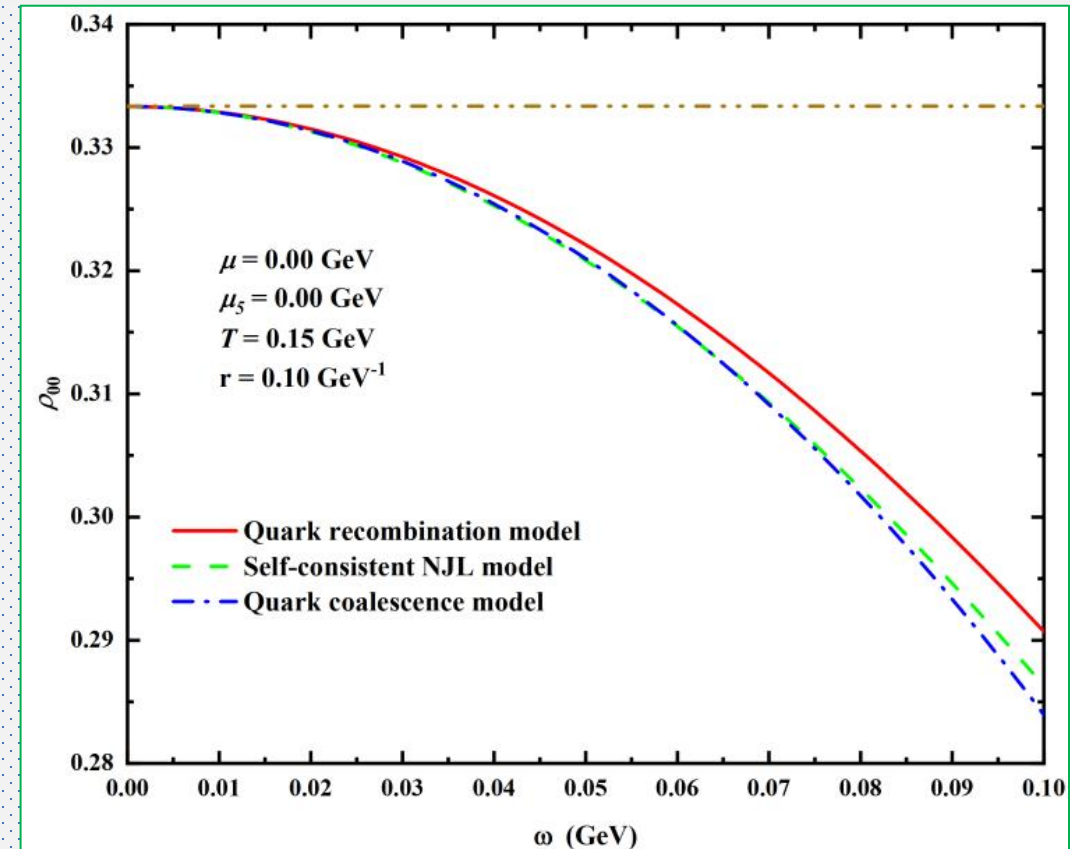
$$\rho_{00} = \frac{1}{3} - \frac{4}{9}(\beta\omega)^2$$

Based on the study of the **self-consistent NJL model [2]**, the spin alignment of vector mesons (including ρ and ϕ) ($T = 150$ MeV), exhibits the following relationship:

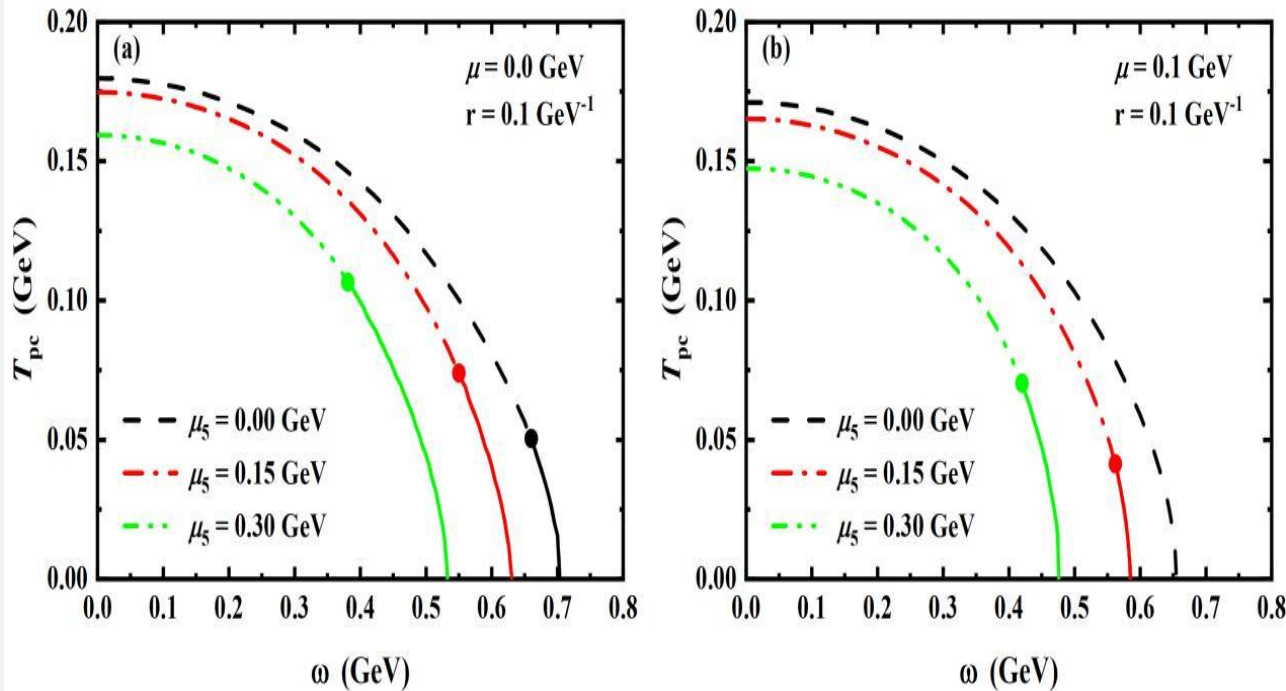
$$\rho_{00} = \frac{1}{3} - 5.10\omega^2 + 39.62\omega^4$$

[1] Y.-G. Yang, R.-H. Fang, Q. Wang, and X.-N. Wang, Phys. Rev. C **97**, 034917(2018).

[2] M. Wei and M. Huang, Chin. Phys. C **47**, 104105(2023).



The phase diagram $T_{\text{pc}} - \omega$ with chiral chemical potential



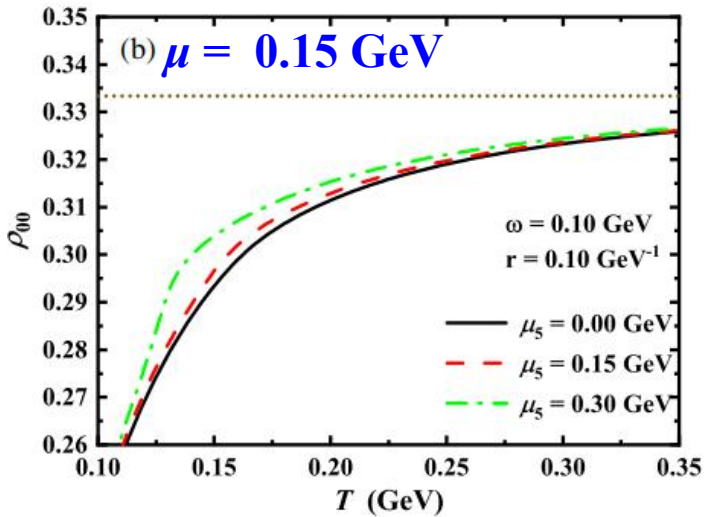
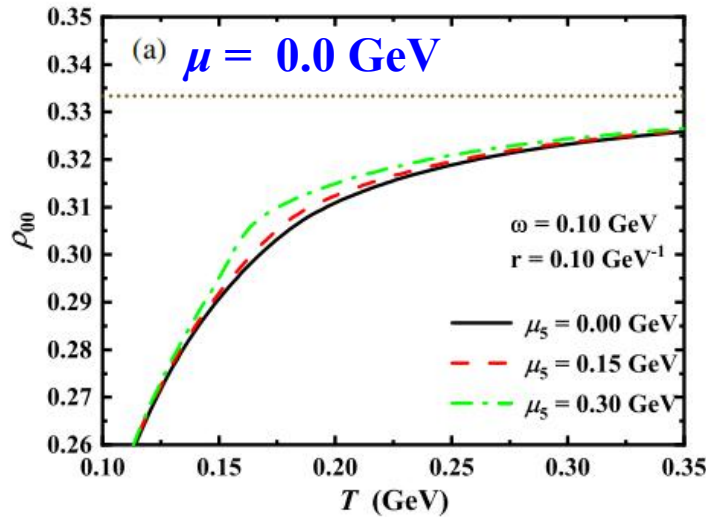
This figure illustrates the chiral phase diagram in the $T_{\text{pc}} - \omega$ plane for varying chiral chemical potentials μ_5 . The critical temperature T_{pc} decreases with increasing μ_5 , and the critical end point (CEP) shifts toward higher T and lower ω .

This is the first study to systematically explore how chiral imbalance (via μ_5) modifies the phase structure of a rotating QCD medium. It uniquely demonstrates that μ_5 suppresses T_{pc} while enhancing the CEP temperature, revealing a competition between rotation and chiral imbalance.

It resolves how chiral imbalance alters the order and criticality of the chiral phase transition under rotation, providing insights into the interplay of vorticity and parity violation in quark-gluon plasma (QGP).

[1] Yang Hua (华杨) and S.-Q. Feng, Phys. Rev. D 111, 036012 (2025).

The relationship between spin alignment ρ_{00} and temperature T



Spin alignment ρ_{00} of ρ mesons as a function of temperature T

Research Content: ρ_{00} approaches $1/3$ (isotropic spin alignment) at high T , while deviating near the phase transition temperature.

Increasing μ_5 enhances ρ_{00} , reducing spin polarization.

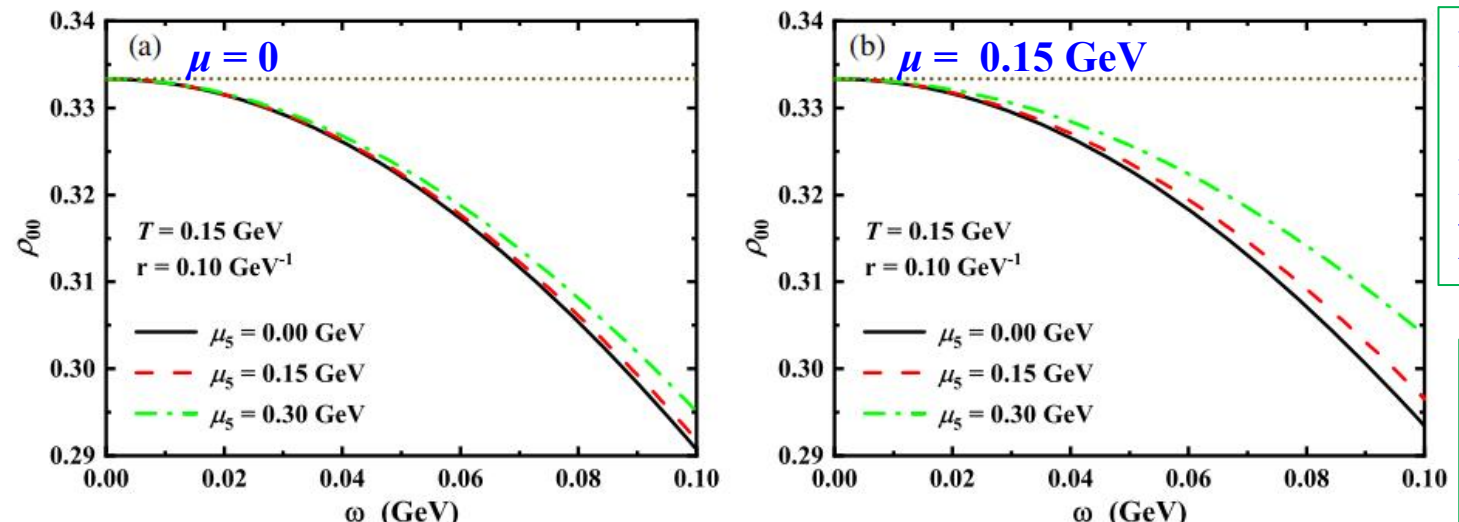
Innovation & Impact: This is the first work to connect chiral imbalance (μ_5) with vector meson spin alignment, showing that μ_5 counteracts rotation-induced polarization near T_{pc} .

Key Problem Solved: It explains how chiral imbalance moderates spin polarization in a temperature-dependent manner, crucial for interpreting experimental ρ_{00} data in QGP.

References:

- [1] Z.-T. Liang and X.-N. Wang, Phys. Rev. Lett. 94, 102301 (2005);
- [2] Z.-T. Liang and X.-N. Wang, Phys. Lett. B 629, 20 (2005).
- [3] Yang Hua (华杨) and S.-Q. Feng, Phys. Rev. D 111, 036012 (2025).

The relationship between spin alignment ρ_{00} and rotational velocity ω



Spin alignment ρ_{00} of ρ mesons as a function of ω

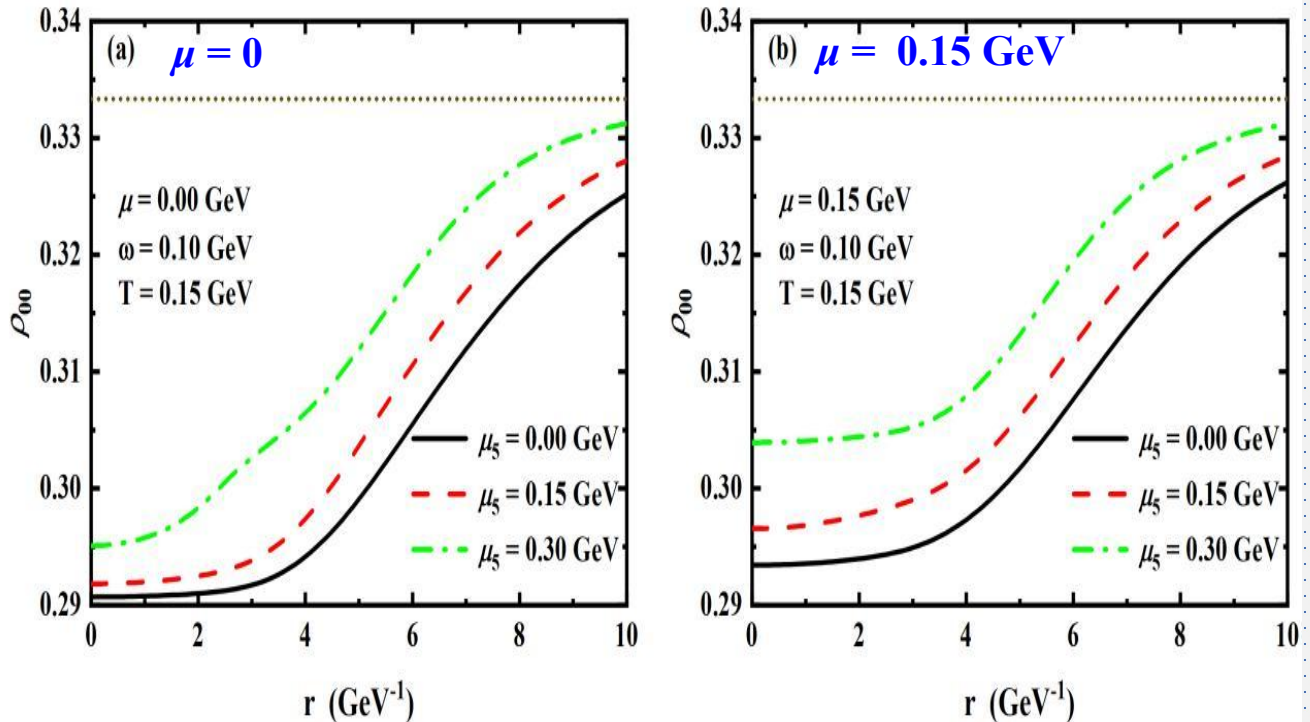
Research Content: ρ_{00} decreases with ω , deviating from 1/3 (indicating polarization). Larger μ_5 reduces this deviation, particularly at high ω .

Innovation & Impact: It demonstrates that chiral imbalance suppresses rotation-induced spin polarization, offering a mechanism to tune meson spin states via μ_5 .

Key Problem Solved: It resolves how competing effects of rotation and chiral imbalance determine the net polarization of vector mesons, vital for probing spin-orbit coupling in QCD matter.

Yang Hua (华杨) and S.-Q. Feng, Phys. Rev. D 111, 036012 (2025).

The relationship between spin alignment ρ_{00} and rational radius



Spin alignment ρ_{00} of ρ mesons as a function of radius r

Research Content: ρ_{00} increases with r , approaching $1/3$, showing reduced polarization away from the rotation center. μ_5 enhances ρ_{00} at all r , especially near T_{pc} .

Innovation & Impact: This study pioneers the spatial analysis of spin alignment in rotating systems, revealing radial gradients in polarization and the moderating role of μ_5 .

Key Problem Solved: It identifies the spatial inhomogeneity of spin polarization in vortical QGP, essential for understanding local spin dynamics in finite-size systems like heavy-ion collisions.

Yang Hua (华杨) and S.-Q. Feng, Phys. Rev. D 111, 036012 (2025).

2. Anomalous Magnetic Moment (AMM) and Neutral Pseudoscalar Meson Dynamics in Magnetized QCD Matter

Based on:

- (1) X.-Q. Zhu (朱学强) and S.-Q. Feng, Phys. Rev. D **107**, 016018 (2023);
- (2) Y.-W. Qiu (邱屹威) and S.-Q. Feng, X.-Q. Zhu (朱学强), Phys. Rev. D **108**, 116022 (2023);
- (3) C.-Y. Yang (杨昌勇) and S.-Q. Feng, arXiv:2503.17056. accepted to be published in Phys. Rev. D.

Main research content and objectives

The research investigates the impact of the anomalous magnetic moment (AMM) of quarks on the mass spectra of neutral pseudoscalar mesons (π , K , η , η') under conditions of strong magnetic fields, finite temperatures, and chemical potentials, based on the three-flavor Nambu-Jona-Lasinio (NJL) model.

The primary research objectives include:

1. **Regulation of quark mass by AMM:** Reveal how AMM alters the variation of quark mass with magnetic field, especially the non-monotonic behavior and first-order phase transition of light quarks (u/d) under critical magnetic fields.
2. **Reconstruction of the QCD phase diagram:** Clarify the influence of AMM on the phase transition temperature (T_c) and critical endpoint (CEP), and explain the consistency between the inverse magnetic catalysis (IMC) effect and the lattice QCD (LQCD) results.
3. **Non-perturbative effects in meson dynamics:** Analyzing how AMM leads to abrupt changes in the mass and stability of neutral pseudoscalar mesons through flavor mixing and chiral symmetry restoration.
4. **The bridging role between theory and experiment:** verifying the necessity of AMM in explaining IMC within an effective model, and narrowing the prediction discrepancies between the NJL model and LQCD.

The SU(3) NJL model with quark AMM

Lagrangian density (three flavors, broken isospin symmetry)

$$\mathcal{L}_{NJL} = \sum_{f=u,d,s} \bar{\psi}_f (i\gamma^\mu D_\mu^{(f)} - m_f - \frac{1}{2} e_f \kappa_f \sigma^{\mu\nu} F_{\mu\nu}) \psi_f +$$

Landau gauge $A_\mu = (0, 0, xB, 0)$

M. Strickland, V. Dexheimer, and D. P. Menezes, Phys. Rev.D 86, 125032 (2012).

$$G \sum_{a=0}^8 [(\bar{\psi} \lambda_a \psi)^2 + (\bar{\psi} i\gamma^5 \lambda_a \psi)^2] - K(\det[\bar{\psi}(1 + \gamma^5)\psi] + \det[\bar{\psi}(1 - \gamma^5)\psi])$$

Mean-field approximation:

Thermodynamic potential: $\Omega_{MF} = \Omega_q + 2G(\sigma_u^2 + \sigma_d^2 + \sigma_s^2) - 4K\sigma_u\sigma_d\sigma_s$

where: $\Omega_q = -3 \sum_{f=u,d,s} \frac{|q_f B|}{2\pi} \sum_n \sum_{s=\pm 1} \int \frac{dp_z}{2\pi} [E_{fns} + T \ln(1 + e^{-\frac{E_{fns} + \mu}{T}}) + T \ln(1 + e^{-\frac{E_{fns} - \mu}{T}})]$

Gap eqs: $\partial \Omega_{MF} / \partial \sigma_f = 0 \implies M_f = m_f - 4G\sigma_f + 2K \prod_{f' \neq f} \sigma_{f'}$

minimizing: Ω_{MF}

Chiral condensates: $\sigma_f = \langle \bar{\psi}_f \psi_f \rangle = -\frac{|e_f B|}{(2\pi)^2} \int dp_z \sum_{n,s} \frac{M_f}{E_{fns}} \left(1 - \frac{s\kappa_f e_f B}{M_{nf}}\right) \left(1 - \frac{1}{e^{(E_{fns} - \mu)/T} + 1} - \frac{1}{e^{(E_{fns} + \mu)/T} + 1}\right)$

Energy eigenvalue: $E_{fns} = \sqrt{p_z + (M_{nf} - s\kappa_f e_f B)^2}, M_{nf} = \sqrt{M_f^2 + 2n|e_f B|}$
AMM

The SU(3) NJL model with quark AMM

Transforming the six-fermion interaction into an effective four-fermion

interaction, one obtains:

$$\begin{aligned}\mathcal{L}_{NJL} = & \sum_{f=u,d,s} \bar{\psi}_f (i\gamma^\mu D_\mu^{(f)} - m_f - \frac{1}{2} e_f \kappa_f \sigma^{\mu\nu} F_{\mu\nu}) \psi_f \\ & + \sum_{a=0}^8 [K_a^- (\bar{\psi} \lambda_a \psi)^2 + K_a^+ (\bar{\psi} i\gamma^5 \lambda_a \psi)^2] \\ & + K_{30}^- (\bar{\psi} \lambda_3 \psi) (\bar{\psi} \lambda_0 \psi) + K_{30}^+ (\bar{\psi} i\gamma^5 \lambda_3 \psi) (\bar{\psi} i\gamma^5 \lambda_0 \psi) \\ & + K_{80}^- (\bar{\psi} \lambda_8 \psi) (\bar{\psi} \lambda_0 \psi) + K_{80}^+ (\bar{\psi} i\gamma^5 \lambda_8 \psi) (\bar{\psi} i\gamma^5 \lambda_0 \psi) \\ & + K_{83}^- (\bar{\psi} \lambda_8 \psi) (\bar{\psi} \lambda_3 \psi) + K_{83}^+ (\bar{\psi} i\gamma^5 \lambda_8 \psi) (\bar{\psi} i\gamma^5 \lambda_3 \psi) \\ & + K_{03}^- (\bar{\psi} \lambda_0 \psi) (\bar{\psi} \lambda_3 \psi) + K_{03}^+ (\bar{\psi} i\gamma^5 \lambda_0 \psi) (\bar{\psi} i\gamma^5 \lambda_3 \psi) \\ & + K_{08}^- (\bar{\psi} \lambda_0 \psi) (\bar{\psi} \lambda_8 \psi) + K_{08}^+ (\bar{\psi} i\gamma^5 \lambda_0 \psi) (\bar{\psi} i\gamma^5 \lambda_8 \psi) \\ & + K_{38}^- (\bar{\psi} \lambda_3 \psi) (\bar{\psi} \lambda_8 \psi) + K_{38}^+ (\bar{\psi} i\gamma^5 \lambda_3 \psi) (\bar{\psi} i\gamma^5 \lambda_8 \psi)\end{aligned}$$

Effective coupling constants:

$$K_0^\pm = G \pm \frac{1}{3} K(\sigma_u + \sigma_d + \sigma_s),$$

$$K_1^\pm = K_2^\pm = K_3^\pm = G \pm \frac{1}{2} K \sigma_s,$$

$$K_4^\pm = K_5^\pm = G \pm \frac{1}{2} K \sigma_d,$$

$$K_6^\pm = K_7^\pm = G \pm \frac{1}{2} K \sigma_u,$$

$$K_8^\pm = G \pm \frac{1}{6} K(2\sigma_u + 2\sigma_d - \sigma_s),$$

$$K_{30}^\pm = K_{03}^\pm = \mp \frac{1}{2\sqrt{6}} K(\sigma_u - \sigma_d),$$

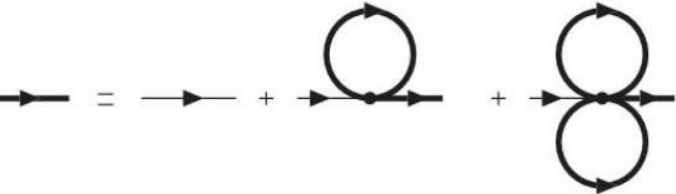
$$K_{80}^\pm = K_{08}^\pm = \pm \frac{\sqrt{2}}{12} K(\sigma_u + \sigma_d - 2\sigma_s),$$

$$K_{83}^\pm = K_{38}^\pm = \pm \frac{1}{2\sqrt{3}} K(\sigma_u - \sigma_d),$$

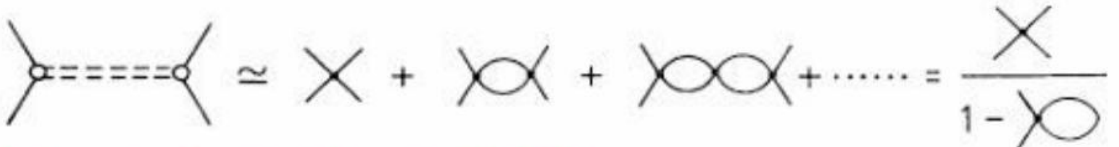
► **Chiral condensates:** $\sigma_u = \langle \bar{\psi}_u \psi_u \rangle, \sigma_d = \langle \bar{\psi}_d \psi_d \rangle, \sigma_s = \langle \bar{\psi}_s \psi_s \rangle$

► Ideas:

(1) Quarks: mean-field



(2) Mesons: RPA resummation (quantum fluctuation)



S. Klevansky, Rev. Mod. Phys. 64, 649 (1992).
M. Buballa, Phys. Rept. 407, 205 (2005).

► Presenting the calculation results directly:

K meson: $M = \frac{2K_6^+}{1 - 2K_6^+ \Pi_{K^0}^{ps}(p)}$

Where

$$\begin{aligned} \Pi_{K^0}^{ps}(p_0 = m_{K^0}) &= \frac{\beta N_c}{2(2\pi)^2} \sum_{n,s,l} \left(1 + sl \frac{M_d M_s + 2\beta n}{M_{nd} M_{ns}} \right) \\ &\times \left\{ \int dk_z \frac{1}{E_{dns}} \left[1 - \frac{1}{e^{(E_{dns}-\mu)/T} + 1} - \frac{1}{e^{(E_{dns}+\mu)/T} + 1} \right] \right. \\ &+ \int dk_z \frac{1}{E_{snl}} \left[1 - \frac{1}{e^{(E_{snl}-\mu)/T} + 1} - \frac{1}{e^{(E_{snl}+\mu)/T} + 1} \right] \\ &\left. + \{[(M_{nd} - s\kappa_d e_d B) - sl(M_{ns} - l\kappa_s e_s B)]^2 - p_0^2\} B(m_d, m_s) \right\} \end{aligned}$$

$$\begin{aligned} B(m_d, m_s) &= \int dk_z \left\{ \frac{1}{E_{dns}} \left[\frac{1}{(E_{dns} + p_0)^2 - E_{snl}^2} \frac{1}{e^{-(E_{dns}+\mu)/T} + 1} \right. \right. \\ &- \frac{1}{(E_{dns} - p_0)^2 - E_{snl}^2} \frac{1}{e^{(E_{dns}-\mu)/T} + 1} \Big] \\ &+ \frac{1}{E_{snl}} \left[\frac{1}{(E_{snl} - p_0)^2 - E_{dns}^2} \frac{1}{e^{-(E_{snl}+\mu)/T} + 1} \right. \\ &\left. \left. - \frac{1}{(E_{snl} + p_0)^2 - E_{dns}^2} \frac{1}{e^{(E_{snl}-\mu)/T} + 1} \right] \right\}. \end{aligned}$$

QCD Phase Diagram Restructuring

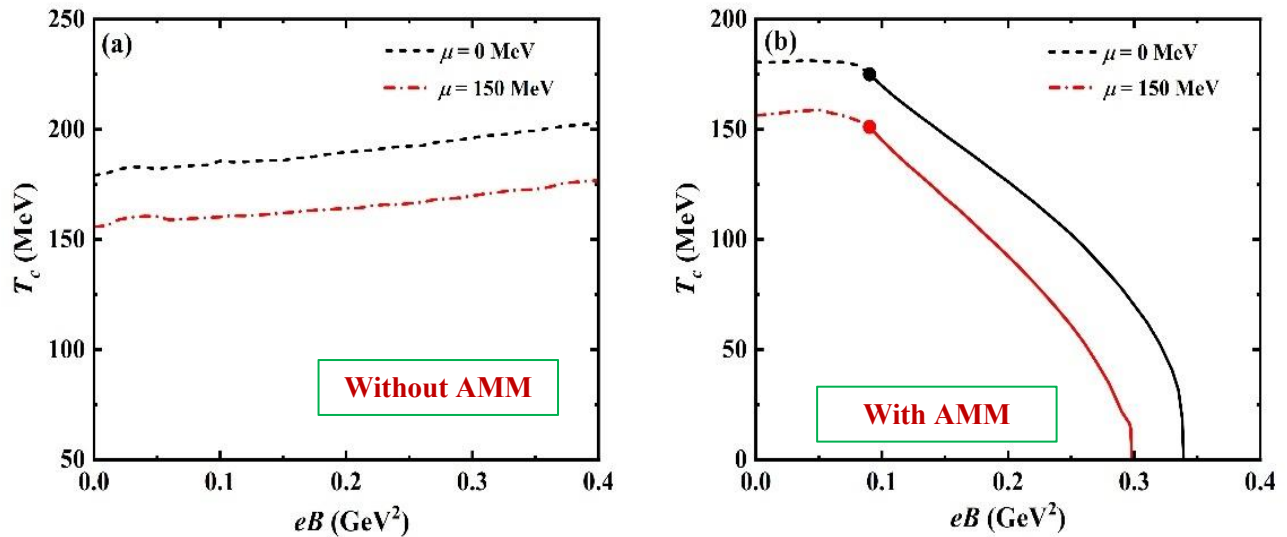


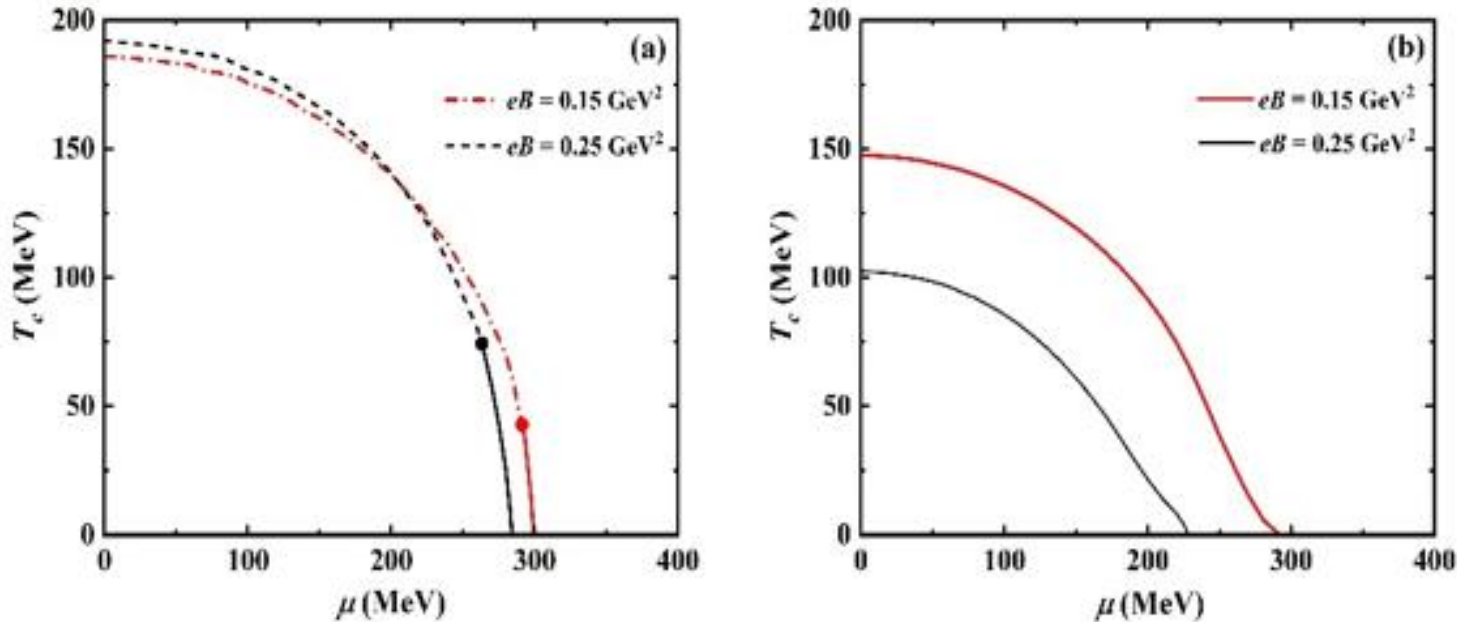
Figure 1 compares the critical temperature (T_c) of chiral phase transitions as a function of eB at different chemical potentials (μ), with and without AMM.

- Magnetic catalysis without AMM
- Inverse magnetic catalysis with AMM
- Non-contradiction with LQCD calculation results.

(1) **Phase Diagram Reshaping and CEP Shift:** AMM suppresses T_c and shifts critical endpoints (CEP) toward lower μ and T , contrasting conventional NJL predictions dominated by magnetic catalysis (MC).
(2) **Crossover-to-First-Order Transition:** AMM replaces crossover transitions with first-order transitions under strong eB , validating AMM's role in altering phase transition sequences in multi-flavor systems.

- (1) X.-Q. Zhu (朱学强) and S.-Q. Feng, Phys. Rev. D **107**, 016018 (2023);
- (2) Y.-W. Qiu (邱屹威) and S.-Q. Feng, X.-Q. Zhu, Phys. Rev. D **108**, 116022 (2023);
- (3) C.-Y. Yang (杨昌勇) and S.-Q. Feng, arXiv:2503.17056. accepted to be published in Phys. Rev. D.

QCD Phase Diagram Restructuring



The critical temperature (T_c) for chiral phase transition as a function of chemical potential for different magnetic fields

- Crossover transitions into first-order transitions without AMM
- Uniform manifestation as first-order phase transitions with AMM
- T_c is a decreasing function of μ

$\mu_{\text{CEP}} \approx 291.2 \text{ MeV}$, $T_{\text{CEP}} = 42.6 \text{ MeV}$ for $eB = 0.15 \text{ GeV}^2$.
 $\mu_{\text{CEP}} \approx 263.3 \text{ MeV}$, $T_{\text{CEP}} = 74.1 \text{ MeV}$ for $eB = 0.25 \text{ GeV}^2$.

- (1) X.-Q. Zhu (朱学强) and S.-Q. Feng, Phys. Rev. D **107**, 016018 (2023);
- (2) Y.-W. Qiu (邱屹威) and S.-Q. Feng, X.-Q. Zhu, Phys. Rev. D **108**, 116022 (2023);
- (3) C.-Y. Yang (杨昌勇) and S.-Q. Feng, arXiv:2503.17056. accepted to be published in Phys. Rev. D.

The magnetic dependences of neutral pseudoscalar meson mass spectra

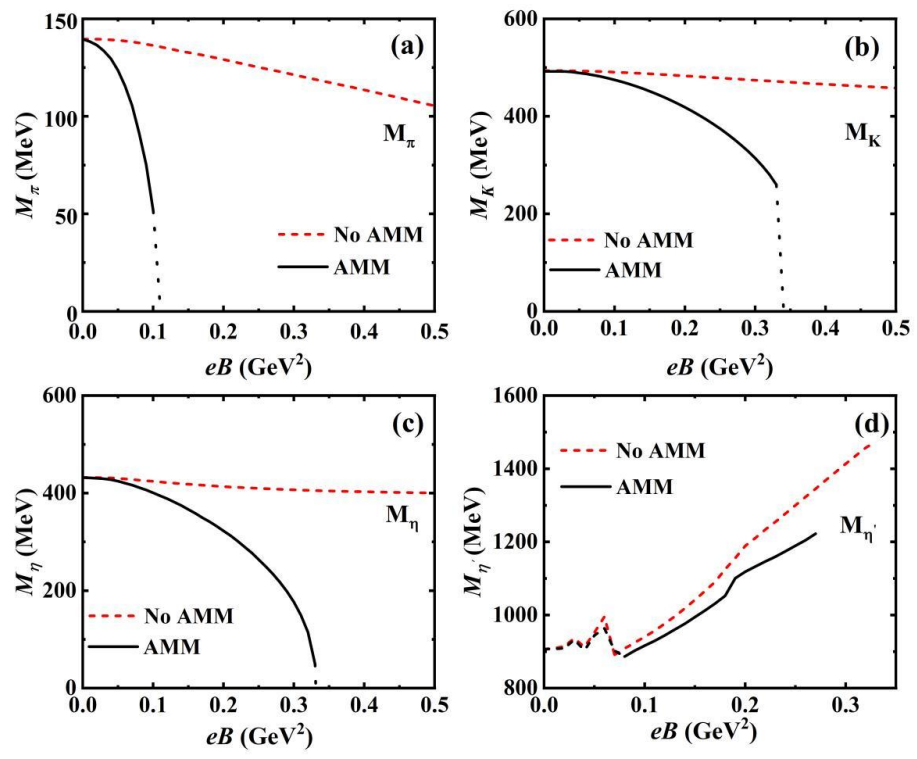


Figure 3 compares the magnetic field dependence of neutral pseudoscalar meson masses (π , K , η , η') at zero temperature, with and without AMM.

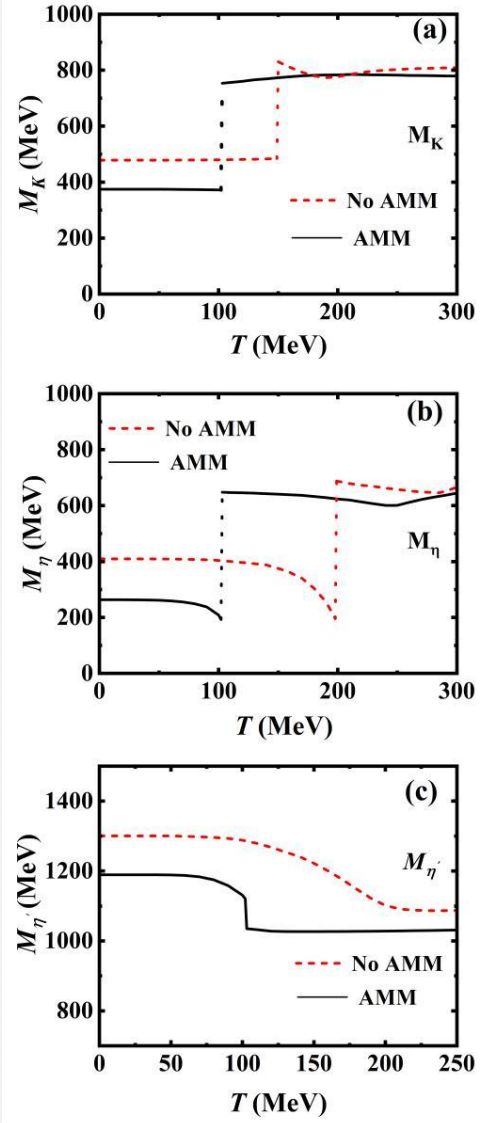
- (1) **Meson Mass Collapse and Chiral Restoration:** AMM triggers abrupt mass collapses (e.g., π at $eB \approx 0.1 \text{ GeV}^2$), directly linking meson stability to chiral symmetry restoration.
- (2) **η' Resonance Limitations:** η' mass diverges under strong eB due to non-perturbative decay width effects, exposing NJL's limitations in handling resonance states.

Key Issues Addressed:

Systematically reveals AMM's role in regulating multi-flavor meson masses and flavor mixing (e.g., π^0 - η - η'), addressing gaps in two-flavor models' predictions for magnetic sensitivity.

- (1) C.-Y. Yang and S.-Q. Feng, arXiv:2503.17056, accepted to be published in Phys. Rev. D

The temperature dependences of neutral pseudoscalar meson masses



● K meson: $T_{mott} \approx 149$ MeV $< T_c \approx 192$ MeV without AMM

$T_{mott} = T_c \approx 102$ MeV with AMM

T_{mott} with AMM $< T_{mott}$ without AMM

● η meson: $T_{mott} \approx 198$ MeV $> T_c \approx 192$ MeV without AMM

$T_{mott} = T_c \approx 102$ MeV with AMM

T_{mott} with AMM $< T_{mott}$ without AMM

● η' meson: The fastest decline in mass without AMM at

$T = 179$ MeV

The fastest decline in mass with AMM at

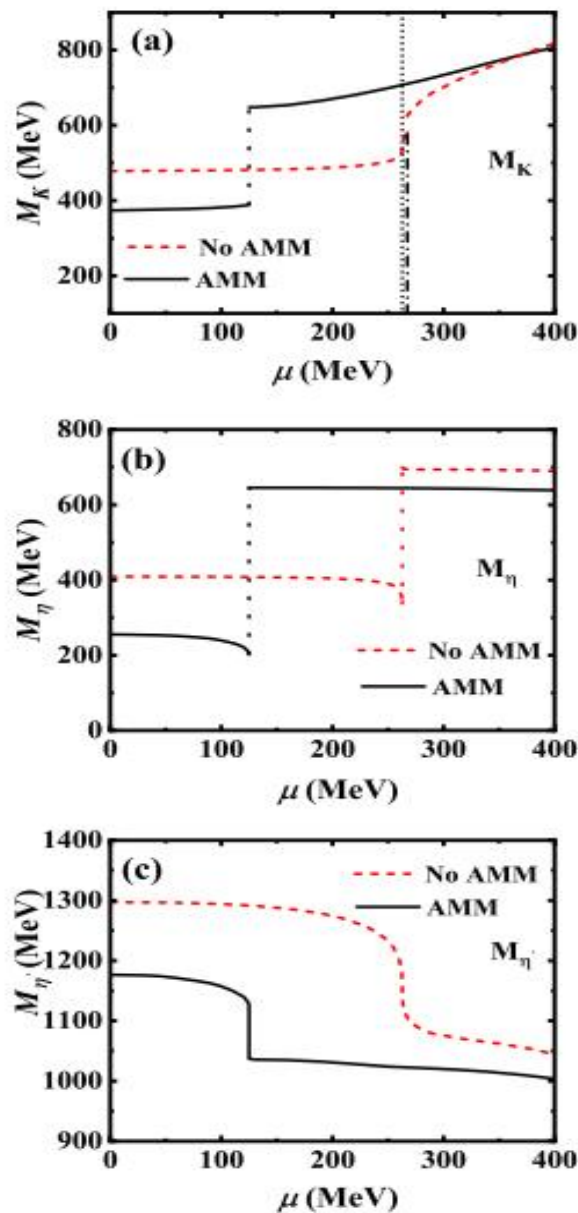
$T = 102$ MeV

Key Issues Addressed:

Demonstrates how AMM-driven quark mass dynamics reshape meson transition pathways, resolving uncertainties in predicting meson stability under high T and B .

(1) C.-Y. Yang and S.-Q. Feng, arXiv:2503.17056, accepted to be published in Phys. Rev. D

The chemical potential dependences of meson mass spectra



- K meson: exhibiting a steep rise in mass at $\mu_{CEP} \approx 262.8$ MeV and a Mott transition at $\mu > \mu_{CEP}$ (discontinuous mass jump) without AMM; a Mott transition happened at $\mu_{CEP} \approx 124.9$ MeV with AMM.
- η meson: exhibiting a Mott transition at $\mu_{CEP} \approx 262.8$ MeV without AMM and at $\mu_{CEP} \approx 124.9$ MeV with AMM.
- η' meson: exhibiting a steep decline in mass at $\mu_{CEP} \approx 262.8$ MeV without AMM and at $\mu_{CEP} \approx 124.9$ MeV with AMM

(1) CEP Relocation: AMM shifts CEP from $\mu \approx 263$ MeV (without AMM) to $\mu \approx 125$ MeV, highlighting AMM's amplification of μ -driven transitions.

(2) Discontinuous Meson Mass Behavior: AMM induces abrupt mass drops at CEP (e.g., K and η meson), linking μ - B synergy to quark mass instabilities.

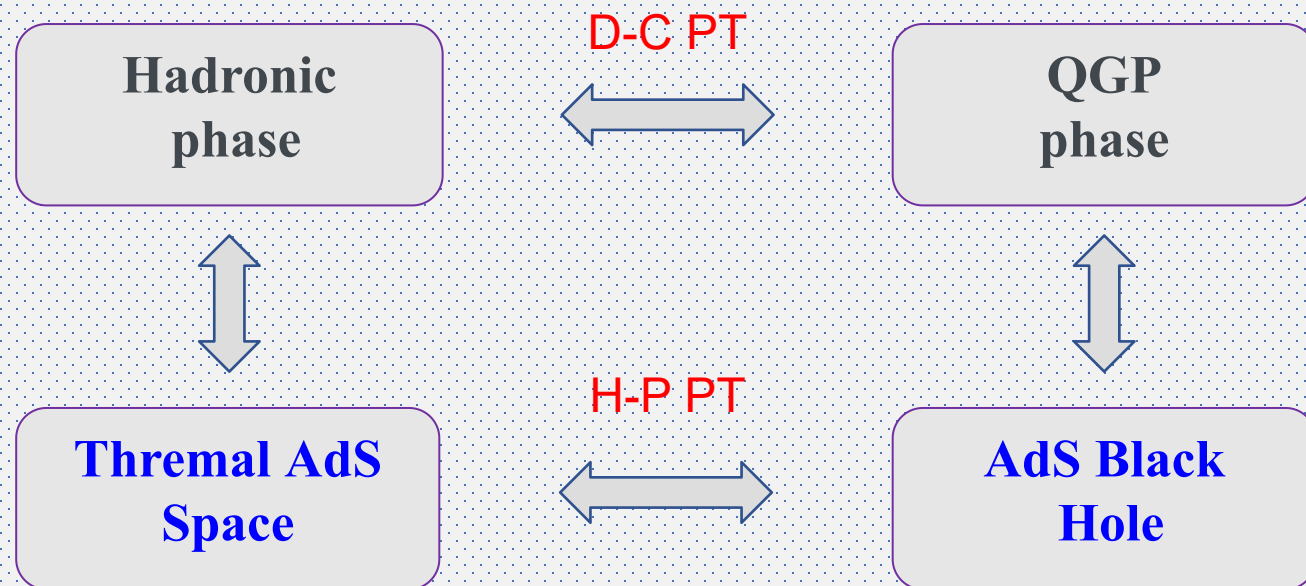
3. Rotation effect on the deconfinement phase transition in holographic QCD

- (1) J.-H. Wang (王嘉豪) and S.-Q. Feng, Phys. Rev. D **109**, 066019 (2024)
- (2) Jiali Deng (邓家力) and S.-Q. Feng, Phys. Rev. D **105**, 026015 (2022)

Hawking-Page Phase Transition

Confinement-Deconfinement Phase Transition in AdS/QCD

E. Witten, Adv. Theor. Math. Phys. 2, 505 (1998).



Research method

Holographic QCD: The holographic principle is used to study the phase transition of QCD, especially through the Einstein-Maxwell system.

Introducing the rotating metric: By introducing a metric with a rotating cylindrical coordinate system, we calculate the Hawking temperature and study the effect of rotation on phase transitions.

- [1] Jia-Hao Wang (王嘉豪) and S.-Q. Feng, Phys. Rev. D **109**, 066019 (2024);
- [2] Jia-Li Deng (邓家力) and S.-Q. Feng, Phys. Rev. D **105**, 026015 (2022)

Introduction of rotation effect

J.-H. Wang (王嘉豪) and S.-Q. Feng, Phys. Rev. D **109**, 066019 (2024); Jiali Deng (邓家力) and S.-Q. Feng, Phys. Rev. D **105**, 026015 (2022)

The rotating extension from the static configuration can be obtained through a **local Lorentz boost** as:

$$t \rightarrow \frac{1}{\sqrt{1-l^2\omega^2}}(t+l^2\omega\phi) \quad \phi \rightarrow \frac{1}{\sqrt{1-l^2\omega^2}}(\phi+\omega t)$$

The corresponding transformation of the metric is:

$$ds^2 = g_{tt}dt^2 + g_{t\phi}dtd\phi + g_{\phi t}d\phi dt + g_{\phi\phi}l^2d\phi^2 + g_{zz}dz^2 + g_{xx}\sum_{i=1}^2dx_i^2$$

To obtain the Hawking temperature of **rotating black hole**, we reestablish the above metric as:

$$ds^2 = \frac{L^2}{z^2} \left[-N(z)^2 f(z)dt^2 + \frac{dz^2}{f(z)} + R(z)(d\phi + P(z)dt)^2 + \sum_{i=1}^2 dx_i^2 \right]$$

$$T_H = \frac{N(z_h)f'(z_h)}{4\pi}$$
$$\mu = \mu' \sqrt{1-\omega^2}$$

The free energy density difference

The action for soft wall model

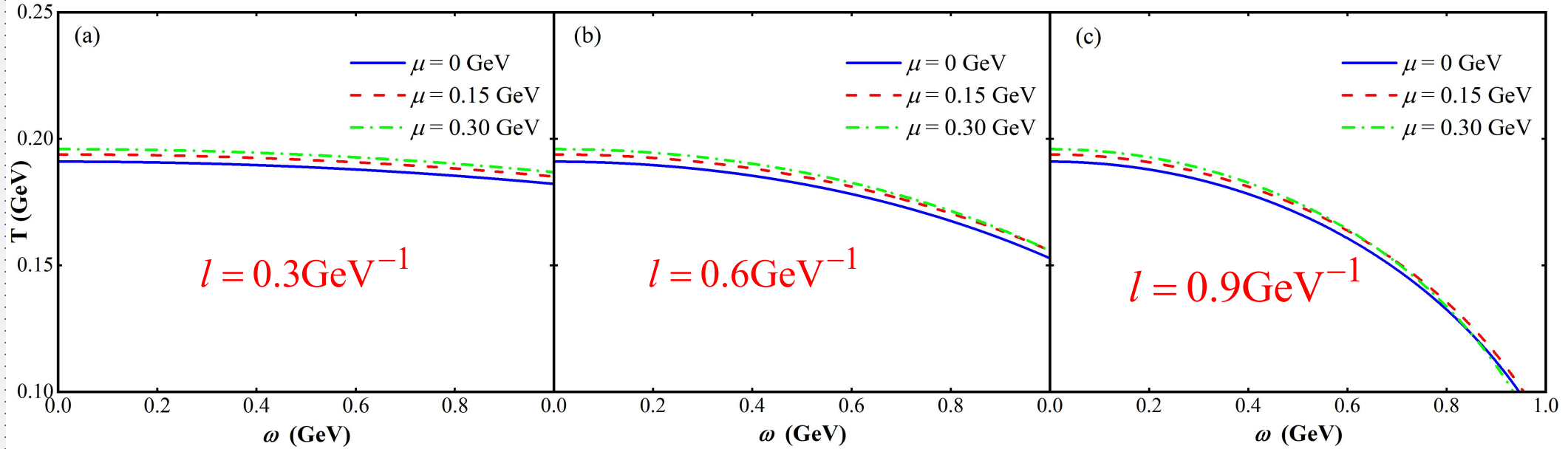
$$S = \int d^5x \sqrt{G} e^{-\Phi} \left[\frac{1}{2\kappa^2} (-R + 2\Lambda) + \frac{1}{4g^2} F_{MN} F^{MN} \right]$$

The free energy density **difference** between the two geometrical backgrounds is

$$\begin{aligned} \Delta F &= T \Delta \mathcal{E} \\ &= \frac{1}{24c\pi^2 z_h^4 (-1 + \omega^2)} e^{-cz_h^2} N_c \\ &\quad (4(-1 + e^{cz_h^2}) N_f \mu^2 - 2c e^{cz_h^2} N_f \mu^2 z_h^2 \\ &\quad + 3c(-2 + e^{cz_h^2}) N_c (-1 + \omega^2) - 6c^2 z_h^2 (N_c + \frac{3}{2} e^{cz_h^2} N_f z_h^2 \mu^2 - N_c \omega^2)) \\ &\quad + 6c^3 e^{cz_h^2} N_c z_h^4 (-1 + \omega^2) Ei(-cz_h^2)) \end{aligned}$$

Result for the Phase transitions of rotations

J.-H. Wang (王嘉豪) and S.-Q. Feng, Phys. Rev. D 109, 066019 (2024)



- For small rotation radii, the phase transition temperature slightly decreases with the rotational angular velocity, but as the rotation radius increases, the phase transition temperature rapidly decreases with the rotational angular velocity.
- This study provides a new perspective for understanding the phase transition characteristics with the size of the rotating systems in strongly interacting matter, and may have guiding significance for future experimental observations.

4. Summary and Conclusions

第二十届全国中高能核物理大会(上海), 2025.4.(24 - 28)

总结和结论

1. 利用有效场理论研究了旋转情况手征不平衡情况下， $T - \omega$, $T - \mu$ 的多维相图特征；
2. 研究了旋转情况手征不平衡情况下，自旋排列特征，分析矢量介子的自旋极化特征；
3. 在三味NJL模型中，研究了强磁场情况下，引入反常磁矩AMM，研究了 $T - \omega$, $T - \mu$ 的多维相图特征，发现反常磁矩改变了相图特征，并且给出的反磁催化特征与格点QCD结果保持一致；
4. 在三味NJL模型中，研究了强磁场情况下，引入反常磁矩AMM，研究了中性赝标量介子质量谱随温度和磁场的变化特征，发现引入AMM对质量谱有显著的影响，改变了传统的NJL模型预言的质量谱与格点QCD结果不一致特征；
5. 本文首次建立了关于均匀旋转系统半径对相图影响的全息研究。由于我们讨论的是QCD介质的旋转系统，相变特性应依赖于旋转系统的有限大小。由于旋转系统具有圆柱对称性，旋转半径r已成为旋转系统的重要特征量。

Thanks !

第二十届全国中高能核物理大会(上海), 2025.4.(24 - 28)